

Contrast Source Inversion Enhanced Confocal Imaging for Highly Heterogeneous Breast Media in Microwave Mammography

Gaku Umezu, Yoshihiro Yamauchi, and Shouhei Kidera , *Senior Member, IEEE*

Abstract—This study introduces accuracy-enhanced confocal imaging (CI) algorithm for highly heterogeneous breast media that can be used in microwave mammography. In the presence of heterogeneous backgrounds, such as breast media, CI accuracy highly depends on several background assumptions, such as homogeneity, multilayered structure, and adipose-dominant tissue. In the case of a highly dense breast dominated by fibroglandular tissue, the traditional CI suffers from inaccuracy due to a large discrepancy between the actual and assumed backgrounds. In this study, we used contrast source inversion (CSI) known as a promising inverse scattering approach, which could provide an accurate estimation of total fields in the region of interest. This feature enables us to generate accurate propagation models as the Green's functions. The numerical tests using realistic breast phantoms show that our method significantly enhances reconstruction accuracy without any prior knowledge of the background media, thus highly contributing to cancer tissue detection.

Index Terms—Confocal imaging, contrast source inversion (CSI), inverse scattering analysis, microwave ultra wide-band (UWB) breast cancer detection.

I. INTRODUCTION

ACCORDING to World Cancer Research Fund International [1], breast cancer is one of the most fatal and diagnosed lesions, but its examination rate is significantly lower than those of other lesions. This is because X-ray mammography, the main screening modality for breast cancer, requires high breast compression and exposure of healthy cells to high energy levels. A few alternatives to this modality exist, such as ultrasonic tomography [2]. However, difficulties remain in recognizing cancerous tissue from dense breast tissue dominated by glandular tissue.

Microwave imaging is a possible solution to the above difficulties, which provides a significant advantages, such as non-contact, less painful, and less cell harmful measurement. Thus,

Manuscript received 10 April 2022; revised 20 June 2022 and 24 July 2022; accepted 31 July 2022. Date of publication 11 August 2022; date of current version 24 November 2022. This work was supported in part by JSPS, in part by KAKENHI under GrantJP20H02161, in part by Prof. S. C. Hagness, in part by the members of the University of Wisconsin Cross-Disciplinary Electromagnetics Laboratory, and in part by the in-house FDTD simulation code. (*Corresponding author: Shouhei Kidera.*)

The authors are with the Graduate School of Informatics and Engineering, The University of Electro-Communications, Tokyo Chofu 182-8585, Japan (e-mail: umezu.gaku@ems.cei.uec.ac.jp; yamauchi.yoshihiro@ems.cei.uec.ac.jp; kidera@uec.ac.jp).

Digital Object Identifier 10.1109/JERM.2022.3196504

it is expected to boost examination rates, especially among young women. According to the literature [3], [4], microwave mammography has a potential feature for early stage cancer detection within 10 mm size, and it would be a promising tool for adjunct modality, where microwave imaging makes more frequent screening techniques, such as once every few months, which X-ray mammography could not be due to its higher energy exposure.

The non-negligible contrast between normal adipose and cancerous tissues [5], generating a significant backscattering echo, guarantees cancerous tissue recognition. Confocal imaging (CI), particularly, radar or beamforming approaches, is a major imaging technique that processes such back scatterers [6]–[8]; a reflection coefficient profile can be retrieved through coherent integration of measured signals observed by sensors surrounding breast media. This method has a low complexity and achieves accurate reconstruction in limited scenarios, such as those with homogeneous background media or high contrast between cancer tissue and background media (usually dominated by adipose tissue, demonstrating low dielectric properties). However, its reconstruction accuracy is severely downgraded in the case of highly dense breast tissue because the CI method commonly assumes a homogeneous background, resulting in a severe mismatch between actual and numerical propagation models. Although several studies have attempted to improve the propagation models in CI [9], generating an appropriate propagation model without any prior knowledge of such a highly heterogeneous background remains challenging.

Inverse scattering (IS) analysis, also known as the tomographic method, solves domain integral equations to address the aforementioned problem. Despite its difficulty, arising from such characteristics as nonlinear features and ill-posed conditions, many IS methods for breast imaging have been developed [10]–[13]. Contrast source inversion (CSI) schemes have become mainstream IS analysis techniques [14], and have been used for breast cancer imaging [15], [16], because of their distinct advantages over other methods. The critical feature of CSI is that it can avoid iterative use of forward solvers, such as the finite difference time domain (FDTD) method, by optimizing not only contrast functions but also total fields defined at all cell locations in the region of interest (ROI); two DIE equations, namely, state and data equations, are introduced. In the literature [17], the CSI is introduced for objects surrounded by walls, assuming through the wall imaging (TWI) scenario, where the

Green's function of the wall layered medium is given as the initial estimate. However, even with the use of CSI, retrieving a complex permittivity profile for a highly heterogeneous profile is difficult because of the presence of ill-posed conditions. Several studies investigated CI-enhanced IS methods [18], [19]. These approaches reduce the number of unknowns for post IS processing. However, few studies focused on using the IS method to estimate the propagation model, *i.e.*, Green's function, in heterogeneous models to enhance CI performance.

Thus, in this paper, we integrate a CI-based radar approach and CSI-based tomography to generate highly accurate CI images for highly heterogeneous backgrounds. Because CSI can provide an optimization output as the total fields for all cells in the ROI, assuming a specific transmitter, the Green's function from a transmitter to a specific ROI cell and to a receiver can be calculated using the reciprocity theorem. That is, an accurate propagation model will be generated even in the presence of a heterogeneous background by providing a profile with a certain level of accuracy via the initial CSI reconstruction. Some studies have been conducted to investigate the possibility of estimating Green's function for accurate radar imaging, such as in the TWI model [20] to deal with multiple scattering effects. The average permittivity was estimated in the literature [21] according to an image focusing criteria. However, this estimation is inaccurate due to the homogeneous assumption that renders the propagation model inappropriate for the process. The study mentioned above [22] has exploited a linear tomographic approach using transmissive time delays in a bistatic configuration. However, this approach is based on a very simple propagation model, *i.e.*, straight-line propagation in heterogeneous media, and ignores diffraction, refraction, and multiple scattering effects. Another study [23] has applied an exponential range-dependent permittivity model for brain intracranial hemorrhage imaging. Nonetheless, this model did not consider the angular dependence of permittivity, which should be considered in highly heterogeneous breast models. Other types of methods, such as [24], [25], could provide average permittivity of breast, however, these methods are hardly applicable to heterogeneous propagation media, such as those in biological tissue. Therefore, developing an accurate CI image that applies to highly heterogeneous media without using computationally expensive forward solvers is innovative. We demonstrate that our proposed method offers accurate CI images for various types of breasts and clear cancerous responses and locations even in dense breast tissue by performing 2D FDTD numerical tests using realistic, magnetic resonance imaging (MRI)-derived phantoms with high heterogeneity.

II. METHOD

A. Observation Model

The observation model is illustrated in Fig. 1 with assumed 2D breast media. Multiple transmitters and receivers are in the region surrounding the breast media; this region is defined as Ω_S or the observation area; this type of observation geometry has been introduced in many studies such as [6], [7], [18]. The ROI, denoted as Ω_D , includes the whole breast

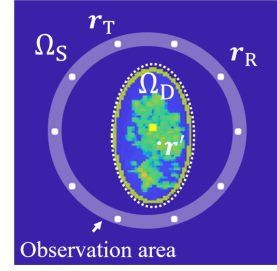


Fig. 1. Observation model. Observation and object areas are defined as Ω_S and Ω_D , respectively. White dots denote the locations of the transmitters or receivers.

area, which is composed of skin, adipose, fibro-glandular, and cancerous tissues, which demonstrate lossy, dispersive, and isotropic dielectric properties. All combinations of transmitters and receivers are used in this observation. $E^T(\omega; r_T, r_R)$ and $E^I(\omega; r_T, r_R)$ are defined as the measured total electric fields with and without the object, respectively, at the receiver, defined as r_R , where the current source is induced at the transmitter as r_T . $E^S(\omega; r_T, r_R) \equiv E^T(\omega; r_T, r_R) - E^I(\omega; r_T, r_R)$ is the scattering electric field.

B. Confocal Imaging Method

The CI is a promising imaging method for microwave breast cancer detection that has been widely applied in numerical and clinical investigations [6], [7]. A distinct advantage of CI is that it can reconstruct the spatial profiles of reflection coefficients with much lower complexity in 3D tissue compared with that required in the tomographic approach. Among various algorithms of the CI, the delay-and-sum (DAS) algorithm is a widely used, where the reconstruction image denoted as $I(r)$ is formulated by the well-known frequency domain expression like [26] as:

$$I(r) = \sum_{(r_T, r_R) \in \Omega_S} \int_{-\infty}^{\infty} E^S(\omega; r_T, r_R) \times G_R^{bg*}(\omega, r, r_R) G_T^{bg}(\omega; r_T, r) d\omega \quad (1)$$

where $*$ denotes the complex conjugate; $G_T^{bg}(\omega; r_T, r)$ denotes the Green's function from the transmitter position r_T to the imaging point r , and $G_R^{bg}(\omega, r, r_R)$ is the Green's function from the imaging point r to the receiver position r_R . Most imaging algorithms introduce the Green's function as:

$$G_T^{bg}(\omega; r_T, r) \simeq \exp\left(j \frac{\omega}{c_{bg}} \|r - r_T\|\right) \quad (2)$$

$$G_R^{bg}(\omega; r, r_R) \simeq \exp\left(j \frac{\omega}{c_{bg}} \|r - r_R\|\right) \quad (3)$$

where c_{bg} denotes the propagation velocity of the assumed background media. In most cases of breast imaging issue, this velocity is calculated from the average relative permittivity of the breast, such as that of adipose tissue, using homogeneous media approximation. The above presumptions are naturally invalid in highly heterogeneous breast media, namely, dense breast. In such cases, the conventional CI method will encounter a

substantial problem; its reconstruction accuracy highly depends on the assumed relative permittivity and will be considerably downgraded due to the above mismatch heterogeneity of the breast.

Numerical solutions have been developed to resolve the above problem, such as the forward solver FDTD. All fields in the ROI are calculated by FDTD, but this approach is impractical because it requires an extremely high complexity and memory.

C. Contrast Source Inversion

We propose solving the above mentioned issue by taking advantage of a distinct feature of CSI, which is a promising IS analysis method. First, the CSI methodology is described as follows: Based on the Helmholtz equations, the scattered electric field $E^S(\omega; \mathbf{r}_T, \mathbf{r}_R)$ is formulated by:

$$E^S(\omega; \mathbf{r}_T, \mathbf{r}_R) = k_{\text{bg}}^2 \int_{\Omega_D} G^{\text{bg}}(\omega; \mathbf{r}, \mathbf{r}_R) w(\omega; \mathbf{r}_T, \mathbf{r}) d\mathbf{r}, \quad (4)$$

where k_{bg} and $G^{\text{bg}}(\omega; \mathbf{r}, \mathbf{r}_R)$ denote the wave number and Green's function, respectively, of the background media. $\chi(\omega; \mathbf{r}) \equiv (\epsilon(\mathbf{r}) - \epsilon_{\text{bg}}(\mathbf{r})) / \epsilon_{\text{bg}}(\mathbf{r})$ is defined as the contrast function, where $\epsilon(\mathbf{r})$ and $\epsilon_{\text{bg}}(\mathbf{r})$ are complex permittivities at the position \mathbf{r} with and without the breast, respectively. $w(\omega; \mathbf{r}_T, \mathbf{r}) \equiv \chi(\omega; \mathbf{r}) E^T(\omega; \mathbf{r}_T, \mathbf{r})$ is the contrast source. In CSI, (4) should be satisfied in both Ω_S and Ω_D . Then, the cost function in CSI is defined considering the two conditions for Ω_S and Ω_D :

$$F(\chi, w) \equiv \frac{\sum_{\mathbf{r}_T} \|E^S(\omega; \mathbf{r}_T, \mathbf{r}_R) - \mathcal{G}^S[w]\|_{\Omega_S}^2}{\sum_{\mathbf{r}_T} \|E^S(\omega; \mathbf{r}_T, \mathbf{r}_R)\|_{\Omega_S}^2} + \frac{\sum_{\mathbf{r}_T} \|\chi(\mathbf{r}) E^I(\omega; \mathbf{r}_T, \mathbf{r}') - w(\omega; \mathbf{r}_T, \mathbf{r}) + \chi(\mathbf{r}) \mathcal{G}^D[w]\|_{\Omega_D}^2}{\sum_{\mathbf{r}_T} \|\chi(\omega; \mathbf{r}) E^I(\omega; \mathbf{r}_T, \mathbf{r}')\|_{\Omega_D}^2}, \quad (5)$$

\mathcal{G}^S and \mathcal{G}^D are defined as:

$$\mathcal{G}^S[w] = k_{\text{bg}}^2 \int_{\Omega_D} G^{\text{bg}}(\omega; \mathbf{r}_R, \mathbf{r}) w(\omega; \mathbf{r}_T, \mathbf{r}) d\mathbf{r}, \quad (\mathbf{r}_R \in \Omega_S), \quad (6)$$

$$\mathcal{G}^D[w] = k_{\text{bg}}^2 \int_{\Omega_D} G^{\text{bg}}(\omega; \mathbf{r}', \mathbf{r}) w(\omega; \mathbf{r}_T, \mathbf{r}) d\mathbf{r}, \quad (\mathbf{r}' \in \Omega_D), \quad (7)$$

$\|\cdot\|_{\Omega_S}^2$ and $\|\cdot\|_{\Omega_D}^2$ denote the l_2 norms calculated in Ω_S and Ω_D , respectively. To minimize its cost function (5), it recursively updates $w(\omega; \mathbf{r}_T, \mathbf{r})$, $E^T(\omega; \mathbf{r}_T, \mathbf{r}_R)$, and $\chi(\omega; \mathbf{r})$. Thus, it reconstructs not only complex permittivity profile but also the total fields of ROI, which can be used to the CI scheme in generating an accurate propagation model.

III. PROPOSED METHOD

By exploiting CSI outputs, we propose the CSI-enhanced CI method, which uses an accurate propagation model, namely, the Green's function, in the presence of a heterogeneous background. The Green's functions used in (1) in the proposed CI scheme, are modified as follows:

$$\tilde{G}_T^{\text{bg}}(\omega; \mathbf{r}_T, \mathbf{r}) \equiv \frac{\hat{E}^T(\omega; \mathbf{r}_T, \mathbf{r})}{E_{\text{bg}}^T(\omega; \mathbf{r}_T, \mathbf{r}_T)} \quad (8)$$

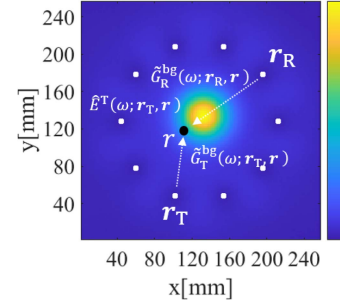


Fig. 2. Total electric field optimized in the CSI and modified Green's functions in the CSI-enhanced CI scheme.

$$\tilde{G}_R^{\text{bg}}(\omega; \mathbf{r}_R, \mathbf{r}) \equiv \frac{\hat{E}^T(\omega; \mathbf{r}_R, \mathbf{r})}{E_{\text{bg}}^T(\omega; \mathbf{r}_R, \mathbf{r}_R)} \quad (9)$$

where $E_{\text{bg}}^T(\omega; \mathbf{r}_T, \mathbf{r}_T)$ and $E_{\text{bg}}^T(\omega; \mathbf{r}_R, \mathbf{r}_R)$ denote the total fields generated by the source located and observed at \mathbf{r}_T and \mathbf{r}_R , respectively where the background media (vacuum) is assumed. Here, $\hat{E}^T(\omega; \mathbf{r}_T, \mathbf{r})$ and $\hat{E}^T(\omega; \mathbf{r}_R, \mathbf{r})$ denote the reconstructed total fields at \mathbf{r} by the prior CSI processing, where $\chi(\omega; \mathbf{r})$ is fixed at the breast media without including cancer. Note that, Green's function defined in (8) and (9) can provide accurate propagation models in the assumed heterogeneous breast media because the optimized total fields $\hat{E}^T(\omega; \mathbf{r}_T, \mathbf{r})$ and $\hat{E}^T(\omega; \mathbf{r}_R, \mathbf{r})$ are generated by the heterogeneous breast media without including tumor. Fig. 2 shows a schematic illustration of the proposed method. Based on the reciprocity theorem, $\hat{E}^T(\omega; \mathbf{r}_T, \mathbf{r})$ and $\hat{E}^T(\omega; \mathbf{r}_R, \mathbf{r})$ are available because the transmitters and receivers are convertible. Since the assumption that the initial CSI process provides an appropriate estimate of the dielectric profile of the breast media, the CSI-optimized total fields could offer accurate Green's functions in heterogeneous media. Finally, the enhanced CI image denoted as $\tilde{I}(\mathbf{r})$ is determined as:

$$\tilde{I}(\mathbf{r}) = \sum_{(\mathbf{r}_T, \mathbf{r}_R) \in \Omega_S} \int_{-\infty}^{\infty} E^S(\omega; \mathbf{r}_T, \mathbf{r}_R) \times \tilde{G}_R^{\text{bg}}(\omega; \mathbf{r}_R, \mathbf{r}) \tilde{G}_T^{\text{bg}*}(\omega; \mathbf{r}_T, \mathbf{r}) d\omega \quad (10)$$

While the proposed scheme requires accurate knowledge of the dielectric profile of the breast media in the absence of cancer, if this knowledge is available, the CSI could provide an accurate estimate of the propagation model, enhancing the CI reconstruction accuracy. Fig. 3 shows the process flow of the proposed scheme.

IV. NUMERICAL TEST

A. Numerical Setup

Numerical tests are performed using the dispersive 2D FDTD method as follows. To assess the applicability of the proposed method, four types of realistic, MRI-derived phantoms retrieved from online repositories are investigated: Class 1 (mostly fatty, ID = 012804), Class 2 (scattered fibroglandular, ID = 070604PA1), Class 3 (heterogeneously dense, ID = 062204),

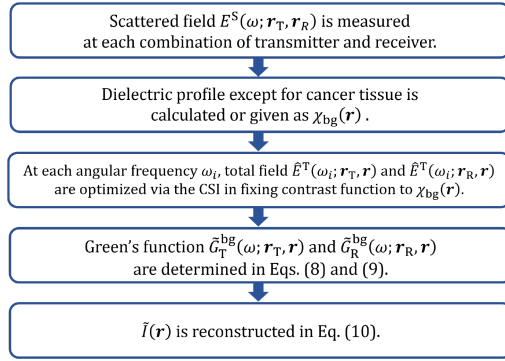


Fig. 3. Processing of the proposed method.

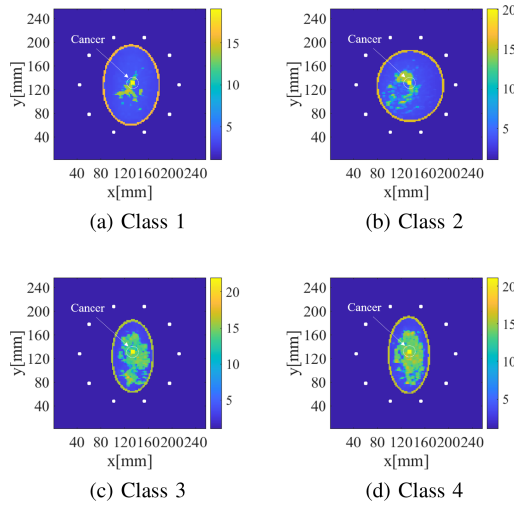

 Fig. 4. Ground truth profiles of Debye parameters ϵ_∞ in each class. White dots denote the transmitters and receivers.

 TABLE I
 DEBYE PARAMETERS FOR EACH TISSUE

Tissue type	ϵ_∞	$\Delta\epsilon$	σ_s [S/m]
Skin	15.93	23.83	0.831
Adipose (median)	3.116	1.592	0.050
Fibroglandular (median)	13.81	35.55	0.738
Fibroglandular (high)	18.3	43.0	1.083
Cancer	22.0	51.6	1.300

and Class 4 (very dense, ID = 012304) [27]. The Debye parameters of each tissue are uniquely associated with the MRI image strength via piece-wise linear mapping [28]. A single-pole Debye model is introduced to express the frequency dependency of each breast tissue; the complex permittivity is expressed as:

$$\epsilon_{\text{Debye}}(\omega; \epsilon_\infty, \Delta\epsilon, \sigma) = \epsilon_\infty + \frac{\Delta\epsilon}{1 + j\omega\tau} + \frac{\sigma}{j\omega\epsilon_0}, \quad (11)$$

where τ is the relaxation time. Fig. 4 shows the spatial profiles of one of the Debye parameters ϵ_∞ in each class, which were retrieved from the MRI images [28]. Table I also shows representative values of the Debye parameters for each tissue, which vary depending on the associated MRI image strength. The maximum

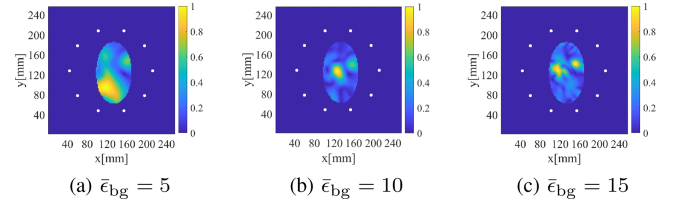


Fig. 5. Reconstruction images by the conventional CI method in Class 3 phantom, with different assumptions of the average relative permittivity of the background.

values are the overall upper bounds, on the frequency-dependent dielectric properties data presented in [5]. Each class includes a cancer tissue at the center of the breast; the tissue is sized 6 mm \times 6 mm and demonstrates Debye parameters $(\epsilon_\infty, \Delta\epsilon, \sigma) = (22.0, 51.6, 1, 3)$, which are approximately 1.2 times larger than those of average fibro-glandular tissues, are available from the phantom repository [27] and [28]. The numbers of transmitters (ideal point sources) and receivers (point sensors), are both 10, and all their combinations are used for the inversion. Note that, reciprocal signals between transmitters and receivers do not contribute any additional information for an inversion, whereas the averaging effect may improve a noise-robust feature using these reciprocal signals. A source excitation current forms a Gaussian modulated pulse with a 2.45 GHz center frequency with a 2.7 GHz bandwidth. The in-house FDTD, which was originally produced by the University of Wisconsin Madison is used. The cell sizes of the FDTD solver, CSI, and CI process are all set to 2 mm, which were obtained by undersampling the original MRI-derived image (resolution = 0.5 mm) using an averaging process. That means that all the Debye parameters of the area defined by 4×4 cells were averaged and allocated to a single 2 mm cell. The heterogeneity of the breast media could then be maintained at a resolution of 2 mm.

Here, two scenarios are investigated to validate the effectiveness of the proposed method. In Case 1, the total fields in the ROI in the presence of cancer tissue (defined as $\hat{E}^T(\omega; r_T, r)$ and $\hat{E}^T(\omega; r_R, r)$ in (8) and (9), respectively) are calculated using the FDTD method, namely, the referential data for the total fields are provided to validate the theoretical correctness of the proposed method. In Case 2, both $\hat{E}^T(\omega; r_T, r)$ and $\hat{E}^T(\omega; r_R, r)$ are optimized through CSI, which is appropriate for practical use. True background Debye profiles except the cancer tissue are given, and the scattered field from this background media is available in both cases.

B. Results and Discussions

First, reconstruction results obtained via conventional CI (Section II-B) from the Class 3 phantom are investigated, as seen in Fig. 5. The different average relative permittivities for the background media are as follows: $\bar{\epsilon}_{\text{bg}} = 5$, $\bar{\epsilon}_{\text{bg}} = 10$, and $\bar{\epsilon}_{\text{bg}} = 15$. The above permittivities are derived from the literature's typical average value of breast media, such as [5], [7]. While fibroglandular permittivity ranges from 40 to 50 at this frequency band, those of adipose tissue ranged from 3 to

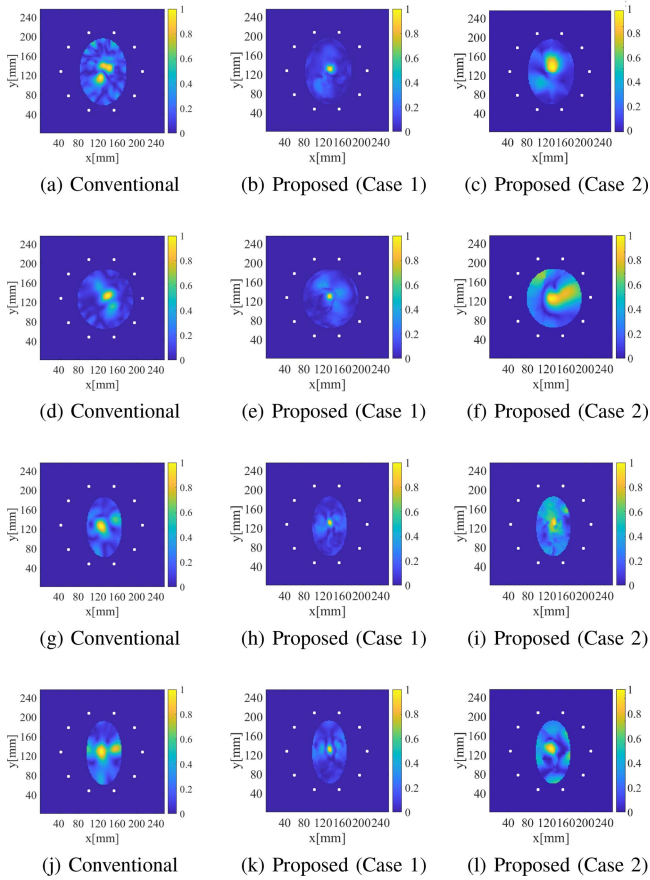


Fig. 6. Reconstruction results of confocal images by each method.

5, and we selected the above permittivity as the representative average permittivity of breast media based on the dominant ratio of adipose tissue. The propagation velocity, defined as c_{bg} , is approximately expressed as $c_{bg} = c_{air}/\sqrt{\epsilon_{bg}}$ in (2) and (3), where c_{air} denotes the propagation speed in the air. As shown in Fig. 5, the reconstruction images significantly depend on the selected relative permittivity, where completely clutter-free scattered data $E^S(\omega; r_T, r_R)$ were input in (1). The case, assuming that $\epsilon_{bg} = 10$, provides relatively more accurate images than other cases. However, these images are coincidentally focused on the center of the breast. A suitable average permittivity is difficult to determine without a prior knowledge of the dielectric properties of the breast because it varies depending on the breast density. Furthermore, even if the SCR is minimal at a specific permittivity, the location of the maximum response would not necessarily indicate the correct location of the cancer tissue. The most critical problem in conventional CI is that the image profile highly depends on the assumed relative permittivity. In addition, conventional CI assumes homogeneous breast media, so unnecessary responses deviated from the cancer position are found despite the complete elimination of backscattered signals.

Next, we show the results obtained by the proposed method in Cases 1 and 2. Fig. 6 shows the reconstruction results for each class by the conventional and proposed methods; according to

TABLE II
SCR IN EACH CASE AND METHOD

	Conventional ($\bar{\epsilon}_{bg} = 10$)	Proposed (Case 1)	Proposed (Case 2)
Class 1	0.4 dB	10.2 dB	6.5 dB
Class 2	4.4 dB	8.6 dB	1.8 dB
Class 3	4.0 dB	9.4 dB	2.4 dB
Class 4	2.8 dB	7.6 dB	3.5 dB

empirical tests, the relative permittivity of $\bar{\epsilon}_{bg} = 10$ is deemed the most appropriate value for the conventional CI technique. For CSI, the iteration number is set to 3,000, and the number of frequency samples is 13, which spans 1.38 GHz to 4.37 GHz with a spacing of 0.23 GHz. As demonstrated in the figure, the most accurate reconstruction is given by the proposed method in Case 1, where all responses are focused on only the cancer tissue's position. By contrast, conventional CI suffers from possibly false positives except for the cancer tissues. This is because the Green's function of the background calculated by the FDTD method can generate an accurate propagation model in the highly heterogeneous, dispersive media. In Case 2, where the Green's function is estimated via CSI optimization, the proposed method provides a certain level of accuracy for reconstructing the cancer tissue. Therefore, the CSI approach can provide an accurate estimate of the Green's function in ill-conditioned scenarios and in the presence of high contrast, dispersive media. However, some unnecessary images or blurred responses are found around the cancer tissue in this case because of either the ill-conditioned problems or the limited iteration numbers. Note that we confirmed that the proposed CI imaging works well when the tumor is located off-center in the breast because it does not require any prior knowledge about an object's location.

The following criteria, such as the SCR, are introduced as quantitative analysis for the CI images and are widely used in CI image assessment [7]. Additionally, the desired CI image should include only responses around the cancer location because each test case includes only one target area (cancer tissue), and the SCR is a suitable metric in this case. Here, the SCR is defined as the power ratio from the first maximum peak to the second maximum peak of an image as follows:

$$SCR = \frac{|I(\hat{r}_1)|}{|I(\hat{r}_2)|} \quad (12)$$

where \hat{r}_i denotes the local maximum points of $|I(r)|$ with the i -th largest strength. Table II compares the SCR values of the conventional and proposed approaches for each case and class, showing that our proposed method achieves significantly higher SCR values in Case 1 by compensating for the propagation model via the FDTD. On the contrary, the SCR values in Case 2 of the proposed method could not retain sufficient improvement from those obtained by the conventional CI. Note that the Euclidean distance between the true cancer position and the maximum point of the CI image is defined as, denoted in [29] because the SCR could not assess the location error of the focal image.

$$Err = \|\hat{p}_{true} - \hat{p}_{CI}\| \quad (13)$$

TABLE III
LOCATION ERRORS Err EACH CASE AND METHOD

	Conventional ($\bar{\epsilon}_{bg} = 10$)	Proposed (Case 1)	Proposed (Case 2)
Class 1	22.7 mm	1.5 mm	3.1 mm
Class 2	4.8 mm	1.2 mm	7.9 mm
Class 3	11.7 mm	0.8 mm	4.3 mm
Class 4	9.5 mm	1.2 mm	3.6 mm

where p_{true} denotes the ground true center position of the cancer and \hat{p}_{CI} expresses the position that has a maximum response of the CI images. Table III shows the Err in each case, and it demonstrates that the proposed method almost retains higher accuracy in both cases compared with those obtained by conventional CI images. In addition, the errors for the images in Fig. 5 are $\text{Err} = 42.3$ mm for the case of $\bar{\epsilon}_{bg} = 5$, $\text{Err} = 11.7$ mm for the case of $\bar{\epsilon}_{bg} = 10$, and $\text{Err} = 20.8$ mm for the case of $\bar{\epsilon}_{bg} = 15$, and these largely depends on the selected $\bar{\epsilon}_{bg}$.

Finally, in this test, we assume that the exact profile of the Debye parameters for background media, namely, the breast without including the tumor, is given to generate the differential signals with and without cancer, however it is rarely available in the actual situation. However, assuming a frequent screening scenario by microwave mammography, it is possible to obtain the scattered data from the healthy state, which would be changed to the malignant state in the future, for the same subject, if that subject is constantly examined by this modality screening. Even if we could not obtain the scattered data from a healthy state, we could obtain a rough estimate of the background media (breast without cancer) using average breast profiles from several subjects. This type of data contains some errors by definition; however, the reconstruction image produced using the proposed method using such a profile could provide more reliable results than the conventional method, assuming a homogeneous background media with an empirically determined relative permittivity. In addition, the response from the breast with no tumors, including skin reflection, was completely subtracted in the simulation test. In the actual measurement scene, the removal of the skin reflection artifact is required. To achieve this, several suppression methodologies [12], [30], [31] have been developed. By providing an accurate background dielectric profile, the above clutter-free signals could be generated by the CSI scheme, especially by using (4). Furthermore, some studies demonstrated that the contrast between cancerous and fibroglandular tissues would be reduced to 10%, which is less than the contrast assumed in this study (20%). In such case, the reflection responses are considerably smaller than those obtained at a contrast of 20%, and the available SNR or SCR could be degraded because it is difficult to completely remove clutters and extract smaller cancer responses. Therefore, further investigations on cases with contrasts of 10% are still required. Since the current study introduces a fundamental solution to this specific problem, there are still some challenges that should be overcome for the practical use of the proposed method. These challenges would be addressed in our future work.

V. CONCLUSION

This paper introduces the CSI-enhanced CI approach for microwave breast cancer detection. The main problem of conventional CI is that its reconstruction accuracy depends on the selected relative permittivity, and it suffers from unnecessary responses because of a mismatch due to the assumed homogeneous media in the propagation model. On the contrary, the proposed method introduces CSI-based Green's function estimation, which is then optimized through CSI iteration. The FDTD method is used to perform numerical analysis in realistic phantoms, and the results show that our proposed scheme provides more accurate CI images by accurately calculating the propagation model in the presence of heterogeneous, dispersive background media. In this test, the Case 1 and 2 are investigated as the proposed method, however, Case 1 needs the FDTD method to generate the Green's function, it is extremely time consuming and requires redundant computation except for the ROI, while, in the Case 2, the CSI provides an minimal requirement data, namely, the total fields in the ROI area for required frequency ranges. Thus, the Case 2 would be more suitable in practical use, while its accuracy depends on the optimization performance of the CSI scheme. Note that, in the numerical test, we give an accurate background breast profile except for the cancer tissue and its subtraction response, which is rarely available in practical scenarios. Nonetheless, this study provides a promising solution to the inherent problem of conventional CI methods, which has never been solved. This study introduces a 2-D numerical test, and an extension to a 3-D model must be included in our future work, where fully polarimetric volume scattering or more complicated multiple reflection effects should be considered. However, the results and discussions of the 2-D model demonstrated in this study are still relevant because major scattering problems, such as multiple scattering effect, frequency dependency, or heterogeneity, have been addressed.

REFERENCES

- [1] F. Bray, J. Ferlay, I. Soerjomataram, R. Siegel, L. Torre, and A. Jemal, "Global cancer statistics 2018: GLOBOCAN estimates of incidence and mortality worldwide for 36 cancers in 185 countries," *Cancer J. Clin.*, vol. 68, no. 6, pp. 394–424, Dec. 2018, doi: [10.3322/caac.21492](https://doi.org/10.3322/caac.21492).
- [2] G. A. G. M. Hendriks, C. Chen, H. H. G. Hansen, and C. L. de Korte, "3-D single breath-hold shear strain estimation for improved breast lesion detection and classification in automated volumetric ultrasound scanners," *IEEE Trans. Ultrason., Ferroelectr., Freq. Control*, vol. 65, no. 9, pp. 1590–1599, Sep. 2018, doi: [10.1109/TUFFC.2018.2849687](https://doi.org/10.1109/TUFFC.2018.2849687).
- [3] B. M. Moloney et al., "Microwave imaging in breast cancer - results from the first-in-human clinical investigation of the Wavelia system," *Acad. Radiol.*, vol. 29, no. Supplement 1, pp. S211–S222, 2022.
- [4] S. Kwon and S. Lee, "Recent advances in microwave imaging for breast cancer detection," *Int. J. Biomed. Imag.*, vol. 2016, 2016, Art. no. 5054912.
- [5] M. Lazebnik et al., "A large-scale study of the ultrawideband microwave dielectric properties of normal, benign and malignant breast tissues obtained from cancer surgeries," *Phys. Med. Biol.*, vol. 52, no. 20, pp. 6093–6115, 2007, doi: [10.1088/0031-9155/52/20/002](https://doi.org/10.1088/0031-9155/52/20/002).
- [6] E. C. Fear, X. Li, S. C. Hagness, and M. A. Stuchly, "Confocal microwave imaging for breast cancer detection: Localization of tumors in three dimensions," *IEEE Trans. Biomed. Eng.*, vol. 49, no. 8, pp. 812–822, Aug. 2002.
- [7] H. Song et al., "Detectability of breast tumors in excised breast tissues of total mastectomy by IR-UWB-radar-based breast cancer detector," *IEEE Trans. Biomed. Eng.*, vol. 66, no. 8, pp. 2296–2305, Aug. 2019.

- [8] A. Naghibi and A. R. Attari, "Near-field radar-based microwave imaging for breast cancer detection: A study on resolution and image quality," *IEEE Trans. Antennas Propag.*, vol. 69, no. 3, pp. 1670–1680, Mar. 2021.
- [9] M. O'Halloran, M. Glavin, and E. Jones, "Improved confocal microwave imaging of the breast using path-dependent signal weighting," in *Proc. XXth URSI Gen. Assem. Sci. Symp.*, 2011, pp. 1330–1334.
- [10] J. D. Shea, P. Kosmas, S. C. Hagness, and B. D. Van Veen, "Three-dimensional microwave imaging of realistic numerical breast phantoms via a multiple-frequency inverse scattering technique," *Med. Phys.*, vol. 37, no. 8, pp. 4210–4226, Aug. 2010, doi: [10.1118/1.3443569](https://doi.org/10.1118/1.3443569).
- [11] L. M. Neira, B. D. Van Veen, and S. C. Hagness, "High-resolution microwave breast imaging using a 3-D inverse scattering algorithm with a variable-strength spatial prior constraint," *IEEE Trans. Antennas Propag.*, vol. 65, no. 11, pp. 6002–6014, Nov. 2017.
- [12] K. Noritake and S. Kidera, "Boundary extraction enhanced distorted born iterative method for microwave mammography," *IEEE Antennas Wireless Propag. Lett.*, vol. 18, no. 4, pp. 776–780, Apr. 2019, doi: [10.1109/LAWP.2019.2902351](https://doi.org/10.1109/LAWP.2019.2902351).
- [13] M. T. Bevacqua, S. Di Meo, L. Crocco, T. Isermia, and M. Pasian, "Millimeter-waves breast cancer imaging via inverse scattering techniques," *IEEE J. Electromagn., RF, Microw. Med. Biol.*, vol. 5, no. 3, pp. 246–253, Sep. 2021.
- [14] P. M. van den Berg and A. Abubakar, "Contrast source inversion method: State of art," in *Prog. Electromagn. Res.*, vol. 34, pp. 189–218, 2001, doi: [10.2528/PIER01061103](https://doi.org/10.2528/PIER01061103).
- [15] H. Sato and S. Kidera, "ROI limited unknowns reduction based contrast source inversion for microwave breast imaging," *IEEE Antennas Wireless Propag. Lett.*, vol. 19, no. 12, pp. 1330–1334, Dec. 2020.
- [16] H. Sato and S. Kidera, "Noise-robust microwave breast imaging applied to multi-frequency contrast source inversion," *IEEE J. Electromagn., RF, Microw. Med. Biol.*, vol. 5, no. 2, pp. 1330–1334, Jun. 2021.
- [17] L. P. Song, C. Yu, and Q. H. Liu, "Through-wall imaging (TWI) by radar: 2-D tomographic results and analyses," *IEEE Trans. Geosci. Remote Sens.*, vol. 43, no. 12, pp. 2793–2798, Dec. 2005.
- [18] M. J. Burfeindt, J. D. Shea, B. D. Van Veen, and S. C. Hagness, "Beamforming-enhanced inverse scattering for microwave breast imaging," *IEEE Trans. Antennas Propag.*, vol. 62, no. 10, pp. 5126–5132, Oct. 2014.
- [19] A. Baran, D. J. Kurrant, A. Zakaria, E. C. Fear, and J. LoVetri, "Breast imaging using microwave tomography with radar-based tissue-regions estimation," *Prog. Electromagn. Res.*, vol. 149, pp. 161–171, 2014.
- [20] P. Setlur, G. E. Smith, F. Ahmad, and M. G. Amin, "Target localization with a single sensor via multipath exploitation," *IEEE Trans. Aerosp. Electron. Syst.*, vol. 48, no. 3, pp. 1996–2014, Jul. 2012.
- [21] B. R. Lavoie, M. Okoniewski, and E. C. Fear, "Estimating the effective permittivity for reconstructing accurate microwave-radar images," *PLoS One*, vol. 11 no. 9, 2016, Art. no. e0160849.
- [22] M. Sarafianou et al., "MUSIC processing for permittivity estimation in a delay-and-sum imaging system," in *Proc. 7th Eur. Conf. Antennas Propag.*, 2013, pp. 839–842.
- [23] A. T. Mobashsher, A. Mahmoud, and A. M. Abbosh, "Portable wideband microwave imaging system for intracranial hemorrhage detection using improved back-projection algorithm with model of effective head permittivity," *Sci. Rep.*, vol. 6, no. 1, 2016, Art. no. 20459.
- [24] O. D. Loughlin et al., "Parameter search algorithms for microwave radar-based breast imaging: Focal quality metrics as fitness functions," *Sensors*, vol. 17, no. 12, 2017, Art. no. 2823.
- [25] J. Bourqui and E. C. Fear, "System for bulk dielectric permittivity estimation of breast tissues at microwave frequencies," *IEEE Trans. Microw. Theory Techn.*, vol. 64, no. 9, pp. 3001–3009, Sep. 2016.
- [26] S. Li, M. Amin, Q. An, G. Zhao, and H. Sun, "2-D coherence factor for sidelobe and ghost suppressions in radar imaging," *IEEE Trans. Antennas Propag.*, vol. 68, no. 2, pp. 1204–1209, Feb. 2020.
- [27] UWCEM, "Numerical breast phantom repository." Accessed: Jul. 15, 2022. [Online]. Available: <https://uwcem.ece.wisc.edu/phantomRepository.html>
- [28] E. Zastrow, S. K. Davis, M. Lazebnik, F. Kelcz, B. D. V. Veen, and S. C. Hagness, "Development of anatomically realistic numerical breast phantoms with accurate dielectric properties for modeling microwave interactions with the human breast," *IEEE Trans. Biomed. Eng.*, vol. 55, no. 12, pp. 2792–2800, Dec. 2008.
- [29] D. Ireland and M. Bialkowski, "Microwave head imaging for stroke detection," *Prog. Electromagn. Res. M*, vol. 21, pp. 163–175, 2011.
- [30] E. J. Bond, X. Li, and S. C. Hagness, and B. D. Van Veen, "Microwave imaging via space-time beamforming for early detection of breast cancer," *IEEE Trans. Antennas Propag.*, vol. 51, no. 8, pp. 1690–1705, Aug. 2003, doi: [10.1109/TAP.2003.815446](https://doi.org/10.1109/TAP.2003.815446).
- [31] H. Song et al., "A two-stage rotational surface clutter suppression method for microwave breast imaging with multistatic impulse-radar detector," *IEEE Trans. Instrum. Meas.*, vol. 69, no. 12, pp. 9586–9598, Dec. 2020.



Gaku Umezu received the B.E. degree in communication engineering and informatics from the University of Electro-Communications, Tokyo, Japan, in 2022.



Yoshihiro Yamauchi received the B.E. degree, in 2021, in communication engineering and informatics from the University of Electro-Communications, Tokyo, Japan, where he is currently working toward the M.E. degree with the Graduate School of Informatics and Engineering.



Shouhei Kidera (Senior Member, IEEE) received the B.E. degree in electrical and electronic engineering, and M.I. and Ph.D. degrees in informatics from Kyoto University, Kyoto, Japan, in 2003, 2005, and 2007, respectively. Since 2009, he has been with Graduate School of Informatics and Engineering, University of Electro-Communications, Tokyo, Japan, where he is currently an Associate Professor. In 2016, he was the Visiting Researcher with Cross-Disciplinary Electromagnetics Laboratory, University of Wisconsin-Madison, Madison, WI, USA. From 2017 to 2021, he was a Principal Investigator with the PRESTO Program of Japan Science and Technology Agency. His current research interests include advanced radar signal processing or electromagnetic inverse scattering issue for ultra wideband 3-D sensor or bio-medical applications. He was the recipient of the 2012 Ando Incentive Prize for the Study of Electronics, 2013 Young Scientists' Prize by the Japanese Minister of Education, Culture, Sports, Science and Technology (MEXT), and 2014 Funai Achievement Award. He is a Senior Member of the Institute of Electronics, Information, and Communication Engineers of Japan (IEICE), a Member of the Institute of Electrical Engineering of Japan (IEEJ), and the Japan Society of Applied Physics (JSAP).